BIOCHEMISTRY
including biophysical chemistry & molecular biology

Article

The Bacteriorhodopsin Carboxyl-Terminus Contributes to Proton Recruitment and Protein Stability

George J. Turner, Shirisha Chittiboyina, Lauren Pohren, Kirk G. Hines, John J. Correia, and Drake C. Mitchell

Biochemistry, **Article ASAP** • DOI: 10.1021/bi801799j

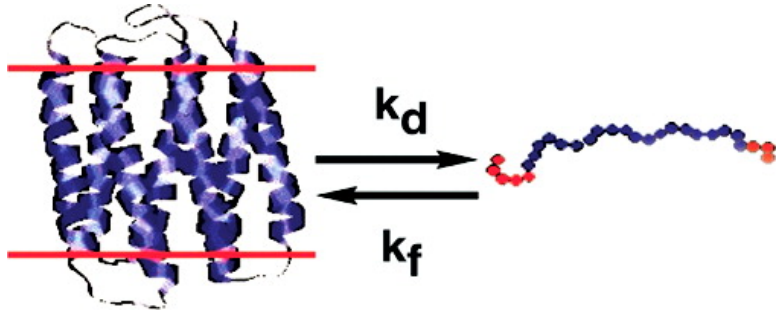

More About This Article

Additional resources and features associated with this article are available within the HTML version:

- Supporting Information
- Access to high resolution figures
- Links to articles and content related to this article
- Copyright permission to reproduce figures and/or text from this article

View the Full Text HTML

Biochemistry is published by the American Chemical Society. 1155 Sixteenth Street N.W., Washington, DC 20036

The Bacteriorhodopsin Carboxyl-Terminus Contributes to Proton Recruitment and Protein Stability[†]

George J. Turner,*[,‡] Shirisha Chittiboyina,[‡] Lauren Pohren,[‡] Kirk G. Hines,[§] John J. Correia,[||] and Drake C. Mitchell[§,⊥]

Department of Chemistry and Biochemistry, Seton Hall University, South Orange, New Jersey 07079, Laboratory of Membrane Biochemistry and Biophysics, NIAAA, NIH, Bethesda, Maryland 20893-9410, Department of Biochemistry, University of Mississippi Medical Center, Jackson, Mississippi 39216, and Department of Physics, Portland State University, Portland, Oregon 97207

Received September 21, 2008; Revised Manuscript Received December 18, 2008

ABSTRACT: We examined functional and structural roles for the bacteriorhodopsin (bR) carboxyl-terminus. The extramembranous and intracellular carboxyl-terminus was deleted by insertion of premature translation stop codons. Deletion of the carboxyl-terminus had no effect on purple membrane (PM) lattice dimensions, sheet size, or the electrogenic environment of the ground-state chromophore. Removal of the distal half of the carboxyl-terminus had no effect on light-activated proton pumping, however, truncation of the entire carboxyl-terminus accelerated the rates of M-state decay and proton uptake ~3.7-fold and severely distorted the kinetics of proton uptake. Differential scanning calorimetry (DSC) and SDS denaturation demonstrated that removal of the carboxyl-terminus decreased protein stability. The DSC melting temperature was lowered by 6 °C and the calorimetric enthalpy reduced by 50% following removal of the carboxyl-terminus. Over the time range of milliseconds to hours at least 3 phases were required to describe the SDS denaturation kinetics for each bR construction. The fastest phases were indistinguishable for all bR's, and reflected PM solubilization. At pH 7.4, 20 °C, and in 0.3% SDS (w/v) the half-times of bR denaturation were 19.2 min for the wild-type, 12.0 min for the half-truncation and 3.6 min for the full-truncation. Taken together the results of this study suggest that the bR ground state exhibits two "domains" of stability: (1) a core chromophore binding pocket domain that is insensitive to carboxyl-terminal interactions and (2) the surrounding helical bundle whose contributions to protein stability and proton pumping are influenced by long-range interactions with the extramembranous carboxyl-terminus.

Bacterio-opsin (Bop[1]) is a 248 amino acid protein that, when coupled to the chromophore *all-trans* retinal, forms the light-activated proton pump bacteriorhodopsin (bR). The proton pumping mechanism involves excitation by light-absorption followed by thermal decay through a series of optically distinct intermediate states (*1, 2*). Transitions between the intermediate state conformations are coupled to protonation and deprotonation reactions, such that each photon absorbed results in a proton being released to the extracellular side (the deprotonation reaction) and a proton being taken up from the intracellular side of the membrane (the reprotonation reaction).

A mechanism for directing protons to the orifice of the cytoplasmic channel in bR has been proposed from structural insight (*3*) and site-directed proton pulsing (*4*). Both studies proposed that a cluster of carboxyls (a "proton antenna") is located in loop regions at the cytoplasmic surface of the channel and that these serve to attract protons from the bulk solution. Interestingly, the extramembranous (and intracellular) bR carboxyl-terminus, composed of amino acids 227−248 (*5, 6*) (Figure 1), contains five carboxylate groups (e.g., three glutamates, one aspartate and the carboxyl-terminal serine). Thus, the bR carboxyl-terminus seemed an intriguing candidate for involvement in proton recruitment.

The bR carboxyl-terminus is disordered and thus invisible to X-ray analysis, thus there can be no structural insight into possible functional or structural roles. Mutagenic analysis of specific amino acids comprising the carboxyl-terminus is sparse; a limited number of site-directed studies have

[†] Support is acknowledged in the form of a Sigrid Juselius Foundation Research Fellowship to G.J.T.

* To whom correspondence should be addressed at The Department of Chemistry and Biochemistry, Seton Hall University, 400 S. Orange Ave., South Orange, NJ 07079. Phone: (973) 761 9598. Fax: (973) 761 9772. E-mail: gturner@mac.edu.

[‡] Seton Hall University.

[§] NIH.

[||] University of Mississippi Medical Center.

[⊥] Portland State University.

[1] Abbreviations: *bop*, bacterio-opsin gene; Bop, bacterio-opsin protein; bR, bacteriorhodopsin; PM, purple membrane harvested from sucrose gradients containing purified bR; PCR, polymerase chain reaction; bp, base pair; SDS, sodium dodecyl sulfate; SDS−PAGE, sodium dodecyl sulfate−polyacrylamide gel electrophoresis; *H. salinarum*, *Halobacterium salinarum*; *E. coli*, *Escherichia coli*; CAPS 3-(cyclohexylamino)-1-propanesulfonic acid; BPT, Bis-Tris-propane, 1,3-bis[tris-(hydroxymethyl)methylamino]propane; LA, light-adapted; DA, dark-adapted; OD, optical density; A_λ, absorbance at wavelength λ; *S*, sedimentation coefficient in Svedberg units; CD, circular dichroism spectroscopy; NMR, nuclear magnetic resonance spectroscopy; FL, fluorescence spectroscopy; EM, electron microscopy; SVD, singular value decomposition; DSC, differential scanning calorimetry; TGAI, bacteriorhodopsin with the twenty-two amino acid carboxyl-terminus deleted; TGAII, bacteriorhodopsin with the distal twelve amino acids of the carboxyl-terminus deleted.

10.1021/bi801799j CCC: $40.75

bop wild-type

```
225 226 227 228 229 230 231 232 233 234 235 236 237 238 239 240 241 242 243 244 245 246 247 248 249
              ≠                                                   ≠
 R   S   R   A   I   F   G   E   A   E   A   P   E   P   S   A   G   D   G   A   A   A   T   S   D
                             §           †                       §                       Δ
cgc agt cgt gcg atc ttc ggc gaa gcc gaa gcg ccg gag ccg tcc gcc ggc gac ggc gcg gcc gcg acc agc gac TGA
                                                                                  Not I
```

bop I

```
cgc agt cgt gcg atc ttc ggc gaa gcc gaa gcg ccg gag ccg tcc gcc ggc gac ggc gcg gcc gcg acc agc gaT TGA
```

bop VIII

```
cgc TCG AgG gcg atc ttc ggc gaa gcc gaa gcg ccg gag ccg tcc gcc ggc gac ggc gcg gcc gcg acc agc gaT TGA
    Xho I
```

bop TGA II

```
cgc TCG AgG gcg atc ttc ggc gaa gcc gaa gcg ccg gag TGA tcc gcc ggc gac ggc gcg gcc gcg acc agc gaT TGA
```

bop TGA I

```
cgc TCG AgG gcg TGA ttc ggc gaa gcc gaa gcg ccg gag ccg tcc gcc ggc gac ggc gcg gcc gcg acc agc gaT TGA
```

FIGURE 1: Bacterio-opsin carboxyl-terminal coding sequences. Shown is the coding region for the extramembranous carboxyl-terminal amino acids 225−249 in the *bop* constructions. Amino acids are numbered and identified by the single letter code. ≠ indicates the truncation sites for the carboxyl-terminal deletions in this study. §, †, and Δ indicate the proteolytic sites (papain, trypsin, and carboxypeptidase A, respectively) used to generate the bR carboxyl-terminal truncation mutants in all previous studies (*11, 41*−*43, 53*−*55*). The shaded amino acid sequence has been proposed to exist as an alpha helical extension of transmembrane helix G (*47*). Nucleotide mutations introduced to remove or introduce DNA restriction sites are designated in capital letters. The C → T mutation in the wobble position coding for D249 removed an endogenous AlwNI DNA restriction site (*24*). Nucleotide changes used to create new DNA restriction sites did not change the resulting amino acid sequence. The cloning sites used to clone the TGA constructions are underlined (*Xho*I and *Not*I). The native translation stop sequence (TGA) is shown in italics. P238 was replaced by the stop codon TGA (bold) to generate bop:TGA II. I229 was replaced by the stop codon TGA (bold) to generate bop:TGA I.

addressed this question (*7*−*9*), as reviewed in ref *10*. The combination of proteolytic deletion and spectroscopic analysis suggested that the carboxyl terminus is segmented into domains with different mobilities and protease susceptibilities (*11*). Proton pumping studies of similarly prepared samples were not conclusive (*12, 13*).

We pursued an alternative strategy that included molecular engineering, spectroscopic, and calorimetric studies to address the potential for carboxyl-terminal amino acids to contribute to bR structure and function. Since the bR carboxyl-terminus contains 25 amino acids, we decided to pursue an efficient low-resolution mutagenic analysis by truncating the bR carboxyl-terminus at two defined locations by the introduction of premature translation stop codons (Figure 1). Removal of the distal half of the carboxyl terminus is referred to as TGAII (TGA is the single letter DNA codon for a translation stop signal) while deletion of all 22 amino acids is referred to as TGAI.

Truncation of the distal portion of the carboxyl-terminus did not affect proton pumping. In contrast, loss of the membrane proximal portion of the carboxyl-terminus perturbed proton recruitment during the time course of M-state decay. Therefore, amino acids in the membrane proximal portion of the carboxyl-terminus must participate in the reprotonation mechanism. Both full- and half-truncation mutants also exhibited reduced stability as measured by SDS denaturation and differential scanning calorimetry. In contrast to studies which indicate bR can functionally tolerate significant deletions and insertions in extramembraneous loop regions (*14*−*18*) our work demonstrates the carboxyl-terminus is required for normal bR structural stability and function.

EXPERIMENTAL PROCEDURES

Microbial Hosts. The *Escherichia coli* strain used was DH5α. *H. salinarum* strains were BopI (*19*) and L33 (*20*).

Media and Growth Conditions. H. salinarum transformation and culturing was accomplished as described (*19, 21, 22*). Selective *H. salinarum* liquid media was supplemented with 10 μM lovastatin (Merck, Sharp and Dohme, Rathaway, NJ). Selective plates included 25 μM lovastatin.

Molecular Reagents. Reagents were obtained from standard molecular biological supply houses. Custom oligodeoxynucleotide primers were purchased from Gibco (Gaithersburg, MD). Oligo-directed mutagenesis was performed with the Transformer Site-Directed Mutagenesis kit, Clontech Laboratories, Inc. (Palo Alto, CA). Electrophoresis grade agarose was from FMC Corporation (Rockland, ME). Nucleotide gel blots utilized Nylon Hybond membranes (Amersham, MA).

bop Gene Constructions. The modifications introduced into the *bop* gene are listed in Figure 1. A unique *Not*I restriction site exists within the carboxyl-terminal coding region of the *bop* gene and was used as the 3′ cloning site. A silent 5′ cloning site (*Xho*I) was introduced into the carboxyl-terminal coding region by oligo-directed mutagenesis and confirmed by DNA sequencing. Subsequent carboxyl-terminal coding regions were constructed from complementary pairs of synthetic oligonucleotides that contained 5′ *Xho*I and 3′ *Not*I DNA restriction sites (Figure 1). Codons 229 (pENDS Bop TGAI) and 238 (pENDS Bop TGAII) were replaced with the translation stop signal, TGA.

H. salinarum expression vectors were constructed by subcloning pENDS vector *Pst*I/*Bam*HI fragments into pHex

vectors (*19*). All pHex vectors were transformed into *H. salinarum* strain L33. Individual transformants were isolated from selective solid media and used to establish 1.5 L cultures (*23*). The *bop* genes containing the TGAII and TGAI mutations were isolated from transgenic *H. salinarum* cells and sequenced, in both orientations, to reconfirm the anticipated mutations. L33 strain expressing pHex Bop I (*19*) was used as a positive control (e.g., wild-type bR).

Protein Purification. Whole membranes were isolated from transgenic cultures as described (*24*). Membrane fractions containing purified bR (the purple membrane, PM) were isolated by sucrose gradient centrifugation (*19, 25*). bR concentration in the PM was quantified using a Perkin-Elmer λ18 spectrophotometer ($\varepsilon^{bR}_{568} = 62{,}700\ M^{-1}\ cm^{-1}$ (*26*)) and LabSphere RSA 150 mm light scattering attachment in the diffuse transmittance mode. The molecular size and purity of the carboxyl-terminally truncated bR's were monitored by SDS−PAGE (NOVEX, San Diego, CA). Unless indicated otherwise, a "standard buffer" (100 mM NaCl, 20 mM CAPS, 20 mM BTP, 20 mM NaH_2PO_4, pH 7.0) was used in all subsequent studies.

Analytical Ultracentrifugation. The sizes of the PM sheets for the wild-type bR and TGAI were determined by sedimentation velocity ultracentrifugation. Samples were spun in a Beckman Optima XLA analytical ultracentrifuge with absorbance optics and an An60Ti rotor at 3 K, 24.7 °C in a charcoal-filled Epon double-sector centerpiece. Samples were equilibrated in standard buffer by passage over a G-50 fine spun column. Data were analyzed with DCDT+ (*27*).

Electron Microscopy. Membrane specimens for electron microscopy were prepared as described (*28*). PM containing the wild-type and carboxyl-terminally truncated bR's, at ~10 μM protein concentration in 10 mM Tris pH 8.0, was spread on an electron microscope grid overlaid with a carbon film, allowed to settle for 90 s and examined in a Philips CM120 electron microscope operated at 100 kV. Images recorded at 45k or 52k magnification and at ~0.5 μm underfocus were screened by optical diffraction.

Circular Dichroism Spectroscopy. Visible CD spectra of samples containing 15 μM protein ($A_{568} = 1.0$) and buffer blanks were measured in 1 cm quartz cells, at 25 °C, in an Applied Photophysics π* CD instrument. Spectra of wild-type bR, TGAII, and TGAI were also collected in the presence of 0.1% Triton X-100 (Pierce) in order to reference the monomeric state spectra (*29*).

Ground-State Spectroscopy. The ground-state spectral properties of wild-type bR and the carboxyl-terminal truncations were compared following light- and dark-adaptation (LA and DA, respectively). 2 μM bR samples were suspended in standard buffer and titrated to pH's 10, 7, and 4 and maintained at 20 ± 0.2 °C. Samples were dark-adapted for 72 h at room temperature and light-adapted by illuminating with >520 nm light for 10 min. The time dependence of DA was recorded on a Perkin-Elmer λ18 spectrophotometer in single wavelength (564 nm) kinetic mode. LA bR (at each pH) was stoppered and the absorbance at 564 nm was recorded at two minute intervals. The membrane samples were continuously stirred to maintain a homogeneous suspension.

Flash Photolysis and Proton Pumping. The kinetics of the M-state formation and decay and the transient release and uptake of protons were measured with a laboratory-constructed flash photolysis instrument previously described (*30*). Excitation was provided by a high-pressure flash lamp (E.G. & G., pulse width = 1 μs) filtered with a broad (±25 nm) band-pass filter centered at 550 nm. In order to improve signal-to-noise, 30 to 50 flashes were averaged together, with no less than 10 s between successive flashes to ensure complete repopulation of the ground state. For M-state measurements samples of 10 μM bR were suspended in standard buffer, and absorbance changes were recorded with matched 410 nm narrow band-pass filters in the monitoring beam. Proton release and uptake were detected in the aqueous bulk medium of the PM suspension using 5 μM fluorescein in unbuffered 100 mM NaCl at pH 7.0. Changes in dye absorbance due to the transient change in pH of the unbuffered medium were obtained by subtracting flash-induced absorbance changes (at 490 nm) observed without the pH indicator dye. Following acquisition of the kinetic data, the pH response of the dye was determined for each sample by using a spectrophotometer to measure the absorbance induced by microliter aliquots of dilute HCl. The resulting calibration curve was used to convert the measured transient changes in fluorescein absorbance into transient changes in proton concentration.

The complete kinetic lifetime of the M-state was analyzed in terms of a coupled double exponential rise and a double exponential decay, with the rise and decay sharing a common amplitude. The flash-induced change in proton concentration in solution was analyzed as a coupled single exponential rise and decay, except for TGAI where analysis of the proton uptake required the sum of two exponentials. All kinetic analysis was performed using NONLIN (*31*) with subroutines specifying the fitting functions written by the authors.

SDS Denaturation. PM, in standard buffer and containing the wild-type bR, and separately the TGAI and TGAII truncation mutants, was mixed with standard buffer plus 0.6% SDS (w/v, Ultrapure, Sigma). The mixing ratio was 1:1 with final protein concentrations ranging from 0.3 to 1.5 μM. The rate constants resolved were independent of protein concentration. All samples and sample compartments were thermally equilibrated at 20 °C. Rapid unfolding events were monitored on a SF-2004 stopped-flow apparatus (KinTek Corp., Austin, TX) with dead time of 0.9 ms. Unfolding was monitored at three wavelengths (568, 400 and 315 nm) in separate experiments. Slower unfolding events were monitored in standard 3 mL quartz mixing cuvettes, and absorbance spectra (250−750 nm) were recorded on an HP 8452A diode array spectrophotometer. Data were analyzed as sums of first order decay reactions. The diode array data were globally analyzed by SVD to kinetic and equilibrium models (Olis Spectral Works). The quality of the kinetic fits was evaluated by randomness of residuals, magnitude of the standard deviations of the fits, and reasonableness of the resolved spectra.

Differential Scanning Calorimetry (DSC). Samples for all DSC measurements were prepared immediately prior to use by suspending purple membrane in pH 7.0, 5 mM phosphate buffer, pelleting at 15,000 rpm in an SS-34 rotor and resuspending in pH 7.0, 5 mM phosphate buffer. This washing procedure was repeated a total of three times. Differential scanning calorimetry measurements were performed with a 6100 Nano-Scan II calorimeter equipped with capillary cells (Calorimetry Sciences, Provo, UT). The

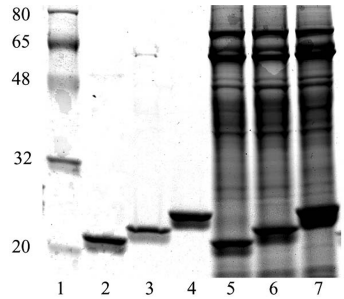

FIGURE 2: SDS−PAGE analysis of bR expression and purification. Equivalent A_{410} of total membrane samples for wild-type bR (lane 7), TGAII (lane 6), and TGAI (lane 5); samples were denatured and electrophoresed. PM samples containing purified wild-type bR (lane 4), TGAII (lane 3), and TGAI (lane 2) were also denatured and electrophoresed. Lane 1 contains molecular size markers (sizes shown in kilodaltons).

sample cell was loaded with 0.21 mg of bR, sealed and maintained at a pressure of 3.0 atm to ensure a stable baseline. Samples were scanned at a rate of 1.5 °C/min from 30 to 110 °C. A second heating scan was repeated after the sample was cooled and equilibrated at 30 °C, and this scan was used to correct for heat capacity changes not related to the protein unfolding transition. DSC scans were normalized to excess molar heat capacity (C_p) using CpCalc 2.1 (Calorimetry Sciences), and the thermograms were analyzed for T_m and ΔH_{cal} using Origin 7 (OriginLab, Northampton, MA) without additional baseline correction. Thermograms were fit using the equation *an asymmetric double sigmoidal in Origin*.

X-ray crystallography. Crystals of TGAI were grown from water−lipid-detergent bicelles (Jaakola and Goldman, manuscript in preparation (*32*)). Data were collected on beamline ID13 at the ESRF.

RESULTS

Protein Expression and Purification. We engineered premature translation stop codons into the *bop* gene carboxyl-terminal coding region to sequentially remove the extramembranous carboxyl-terminus. Truncation of the distal half (TGAII) and entire carboxyl terminus (TGAI) is depicted in Figure 1. PM's containing wild-type and truncated bR were purified via sucrose gradient centrifugation. The PM for each construction banded at the same sucrose density (data not shown), indicating that the lipid "to" protein composition for each construction was similar. SDS−PAGE analysis of whole membrane fractions and purified PM (Figure 2) exhibited a doublet for each construction, due to normal processing of the amino-terminal leader sequence (*33*). As observed previously, the bands corresponding to bR migrated anomalously rapidly (*25, 33*). The differences in mobility observed were consistent with removal of 1,108 daltons (Da) in TGAII and an additional 961 Da in TGAI. Following incubation with *all-trans* retinal, purified PM's showed no increase in absorbance at 568 nm demonstrating that the PM for each truncation was maximally retinylated *in vivo* (data not shown).

Physical Properties. The PM sheet size for both wild-type bR and TGAI was analyzed by analytical ultracentrifugation and electron microscopy. The sheet size distributions determined by ultracentrifugation are broad and peaked at 1200 S for wild-type bR and 1300 S for TGAI bR, with the TGAI

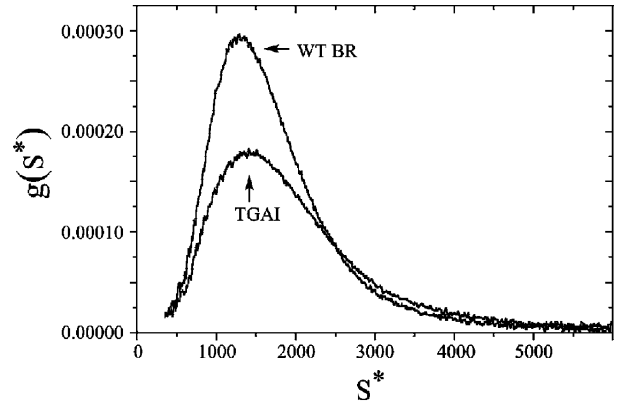

FIGURE 3: PM sheet size determination by ultracentrifugation. Wild-type (top curve) and TGAI (bottom curve) purified PM were equilibrated into pH 7 buffer, and their sedimentation behavior was evaluated by analytical ultracentrifugation. The difference in curve heights corresponds to the total amount of sample used in individual experiments. The sedimentation profiles were monitored at 568 nm, the visible absorbance maximum for bR. The distribution of sedimentation coefficients $g(S^*)$ is plotted versus the sedimentation coefficient, S^*. The distributions are extremely broad and peaked at 1200 S for wild-type bR and 1300 S for TGAI, with TGAI slightly more polydisperse.

sample slightly more polydisperse (Figure 3). While these are obviously large structures (involving 10,000's of bR monomers), there is no significant difference in sheet size distribution and there is no evidence of nonspecific aggregation caused by removal of the carboxyl terminus. The polydispersity of sheet polymers is not unexpected as there are no obvious constraints on extent of growth in any dimension. EM analysis demonstrated that the average size for the PM sheets ranged between 0.4 and 1.2 μm for all samples (data not shown). The optical transform of low-dose pictures of recombinant specimens showed hexagonal patterns analogous to that from wild-type PM with spots going out to ~16 Å resolution, which was within ~4% of that for wild-type PM. This difference was within the error level inherent in this technique (e.g., due to uneven specimen preservation or radiation damage) and suggested that the lattice formed by the deletion constructions was unchanged. The similarities in PM buoyant density, sheet size and lattice dimensions indicated that biogenesis of the PM sheets was not significantly perturbed by truncation of the bR carboxyl-terminus.

Exciton coupling in the visible CD spectrum is characteristic of the trimeric state of bR in the PM lattice (*34, 43*). The visible CD spectral profiles obtained for PM suspensions of wild-type bR and both carboxyl-terminal truncations were indistinguishable (data not shown). In all cases the CD spectra were uncoupled on addition of Triton X-100 (data not shown). In combination with the EM analysis, these observations demonstrated that carboxyl-terminal truncations exist as trimers and the relative orientation of the three retinal chromophores, within the trimer, were indistinguishable from that observed for the wild-type bR.

To determine the effect of the carboxyl-terminal truncation on ground-state absorbance properties, the PM isolated from each construction was examined by UV/visible absorption spectroscopy at pH 10, 7, and 4. For LA wild-type bR the chromophore is 100% in the all-trans configuration while in the DA state an equilibrium mixture of 13-cis (65%) and

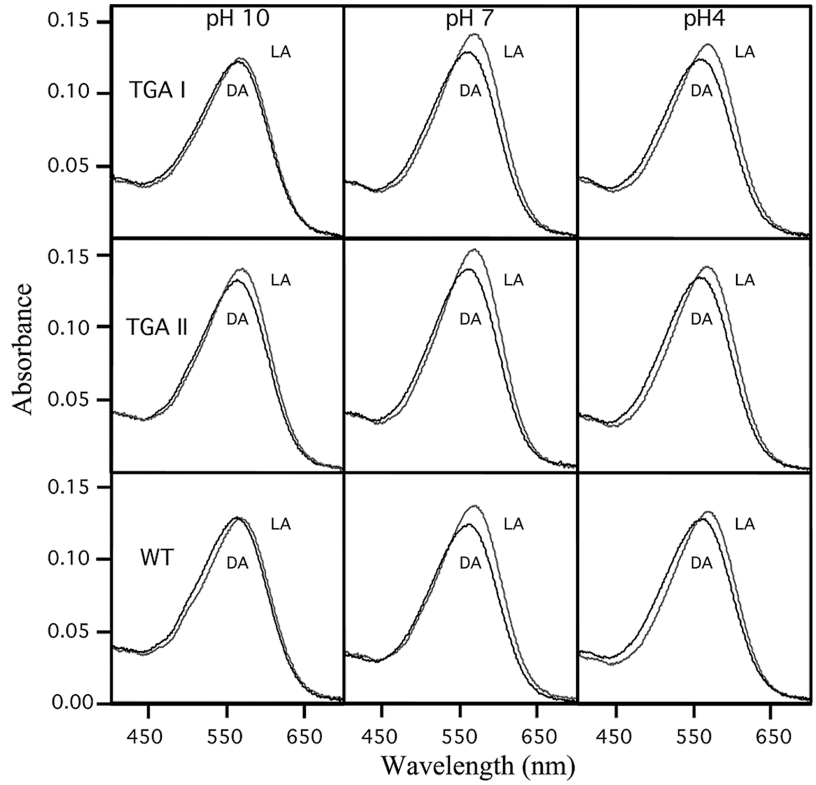

FIGURE 4: pH-dependence of the ground-state spectra for wild-type bR and carboxyl-terminal truncations. Two μM PM samples were suspended in 100 mM NaCl, 10 mM CAPS, 10 mM BTP, 10 mM NaH_2PO_4 and titrated to pH's 10, 7, and 4. Spectra were obtained at 20 °C. Curves: DA, samples were dark-adapted for 4 days at 4 °C; LA, samples were light-adapted by illumination for 30 min (at 20 °C) with >530 nm light.

all-trans (35%) chromophore exists (*35, 36*). Both carboxyl-terminal deletions exhibited normal light- and dark-adapted spectra (Figure 4) with an absorption maximum within 2 nm of wild-type bR at each pH. The time dependence of formation of the dark-adapted state of bR and TGAI was evaluated at pH 7. The rate of dark-adaptation was best described by a single first order process with very similar values for k_{DA} (2.5×10^{-2} min^{-1} for bR and 3.0 x10^{-2} min^{-1} for TGAI, data not shown).

Therefore, there were no gross defects in the electronic environment of the chromophore in the ground state, assembly into trimers, or the aggregation state of the PM following partial or full truncation of the bR carboxyl-terminus.

Proton Pumping. To evaluate the effect of the carboxyl-terminus on bR function, the rates of decay and formation of the M-state and rates of proton release and uptake were evaluated via flash photolysis. The two carboxyl-terminal deletions had very different effects on light-activated proton pumping. Deletion of the distal 11 amino acids from the carboxyl-terminus produced only small changes in the kinetics of M-state formation and decay, and proton release/uptake, as shown by comparing the kinetic traces in Figure 5A with those in Figure 5B. Detailed analysis of the kinetic processes (Table 1) showed that both the M-state formation and decay and proton uptake/release kinetics of TGAII were essentially identical to those of wild-type bR. In contrast, complete deletion of the carboxyl-terminus in TGAI resulted in dramatic changes in the kinetics of both the M-state formation and decay, and proton release/uptake, as shown by comparison of the traces in Figure 5C with those in Figures 5A and 5B. The time constant of M rise was slightly reduced in TGAI, but the average time constant of M decay was reduced by almost a factor of 5 (Table 1). This resulted in a decrease of the apparent amplitude of the M-state (Figure 5C). The time constant of proton release was essentially unchanged in TGAI, but proton uptake was distorted, as shown by the biphasic decay of proton concentration, (Figure 5C). The fast process of proton uptake by TGAI has a time constant of 1.7 $\pm$ 0.1 ms (amplitude of 86%), and the slow process had a time constant of 60 $\pm$ 4 ms (amplitude of 14%).

SDS Denaturation. We compared the rates of unfolding in the presence of 0.3% SDS (w/v) as a measure of potential structural perturbations linked to the loss of carboxyl-terminal amino acids. Upon mixing with SDS, significant decreases in absorbance were observed for all three forms of bR. The spectral changes originated from reduction of scattering upon disruption of the large PM particles and bleaching of the retinal chromophore upon bR unfolding. The short-time scale reactions were evaluated separately at 568 nm (loss of ground-state absorbance as bR unfolds), 400 nm (increase in absorbance as the free retinal is released from the apoprotein) and 315 nm (loss of light scattering as PM particles are solubilized by SDS; there is no retinal component in the optical density of the PM at 315 nm). The initial phases of the denaturation reaction (rates and amplitudes) were indistinguishable at all three wavelengths for the full truncation (TGAI, Figure 6). An identical result was observed for the wild-type bR and TGAII, at all wavelengths monitored (data not shown). In brief, the data were described by a very rapid phase (average $t_{1/2} = 21 \pm 5$ ms) and a second phase (average $t_{1/2} = 1.8 \pm 0.8$ s, Table 2), with very similar amplitudes in all cases. The fast-time scale reactions were

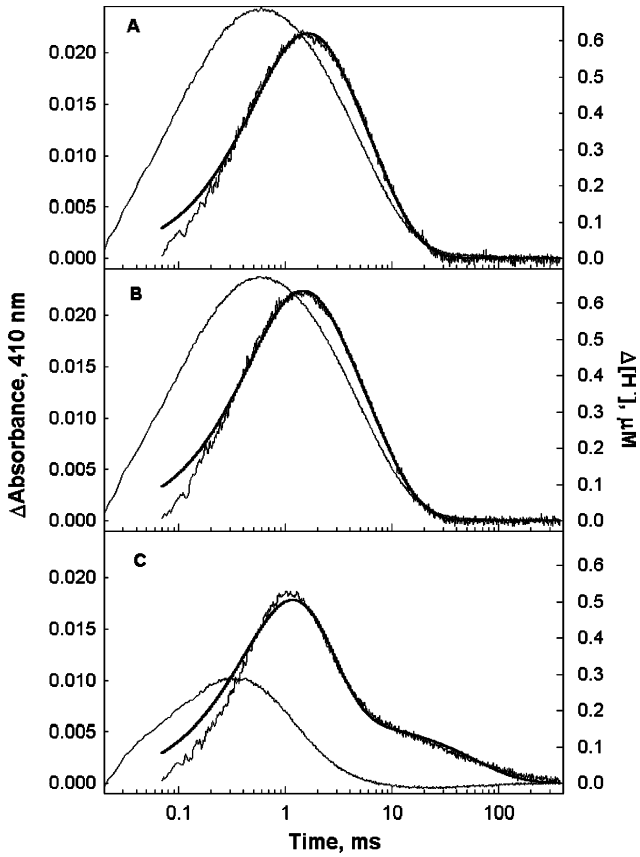

FIGURE 5: Kinetics of M-state formation and decay, and proton release and uptake: (A) wild-type bR; (B) TGAII; (C) TGAI. In each panel the lighter, left-most curve is the flash-induced formation and decay of the M-state observed at 410 nm plotted according to the left axis. The smooth curve through the data shows the results of analyzing the complete kinetic lifetime of the M-state in terms of a coupled double exponential rise and a double exponential decay, with the rise and decay sharing common amplitude. The darker, right-most curve is the flash-induced change in free proton concentration, as reported by the change in fluorescein absorbance (at 490 nm) plotted according to the right axis. The smooth curve through the data shows the results of analyzing the flash-induced change in proton concentration in solution in terms of a coupled single exponential rise and decay, except for TGAI (panel C) where analysis of the proton uptake required the sum of two exponentials. All samples contained 100 mM NaCl, pH 7.0 at 20 °C; samples for M-state measurements also contained pH 7.0 buffer. Changes in proton concentration were derived from the calibrated response of the fluorescein dye as described in the text.

interpreted as losses in light scattering due to SDS:PM interactions. In contrast, the longer-time scale absorbance changes indicated dramatic increases in the apparent rates of unfolding upon removal of the distal and proximal portions of the carboxyl-terminus (Figure 7). For each bR species the SVD global analysis of the diode array spectra was best described by two sequential first order decays. The spectral changes indicated a further loss in the light scattering component and the bR denaturation reaction, with concomitant accumulation of free retinal (Figure 7). The first phase overlapped the second phase of the stopped-flow analysis and hence was associated with loss of light scattering. This phase was not well resolved due to the relatively long mixing times required for the large volume standard mixing cell cuvettes. The spectra resolved from the SVD analysis allowed unambiguous association of the second phase with the bR → bO reaction. The denaturation rates resolved were 2.22 ± 0.09 h^{-1} for the WT, 3.39 ± 0.16 h^{-1} for TGAII, and 10.3 ± 0.70 h^{-1} for TGAI. The kinetic analyses demonstrated that SDS denaturation of bR in the PM was initiated by rapid solubilization of the membrane particles and, the stability of bR was significantly reduced upon removal of carboxyl terminal amino acids.

Table 1: Summary of M-State and Proton Release/Uptake Kinetics

	wild-type	TGAII	TGAI
M rise[a]			
τ(fast)	0.090 ± 0.005	0.094 ± 0.004	0.121 ± 0.002
τ(slow)	0.24 ± 0.02	0.26 ± 0.02	
% fast	58.2 ± 2.5	63.5 ± 3.2	100
$\langle\tau_{rise}\rangle$	0.15 ± 0.01	0.16 ± 0.01	0.12 ± 0.002
M decay[a]			
τ(fast)	4.91 ± 0.06	4.71 ± 0.08	1.29 ± 0.02
τ(slow)	19.5 ± 0.7	14.1 ± 0.8	2.87 ± 0.3
% fast	88.7 ± 1.0	83.2 ± 1.6	91.8 ± 2.2
$\langle\tau_{decay}\rangle$	6.56 ± 0.05	6.29 ± 0.05	1.41 ± 0.02
proton release[b]			
τ	0.64 ± 0.02	0.53 ± 0.02	0.67 ± 0.03
proton uptake[b]			
τ(fast)	6.2 ± 0.1	6.4 ± 0.1	1.7 ± 0.1
τ(slow)			60 ± 4
% fast	100	100	86 ± 2

[a] Time constants in ms and fractional amplitudes resulting from analysis of the M-state in terms of a coupled double exponential for both the rise and decay. [b] Analysis of the changes in dye absorbance due to proton release/uptake as coupled single exponentials. For TGAI accurate description of proton uptake required the sum of two exponentials (see Figure 5C and text).

DSC. The thermal stability of both WT and TGAI were investigated by differential scanning calorimetry, as shown in Figure 8. Under the conditions employed (no salt, 5 mM phosphate buffer, pH 7.0) the low temperature transition ascribed to PM lattice disruption was barely detectable between 60 and 70 °C. As previously demonstrated, the thermal denaturation of bR was irreversible (*37, 38*), so comparison between WT and TGAI was accomplished by scanning at identical rates. The high temperature transitions accompanying bR denaturation (*39*) were well modeled by a single Gaussian indicating that bR−bO reaction is closely approximated by a two-state transition. The temperature at the maximum excess heat capacity, T_m, was sensitive to the absence of the carboxyl-terminus as seen by the reduction from 98.0 ± 0.1 °C for the WT to 92.0 ± 0.1 °C for TGAI. Removal of the carboxyl-terminus also altered the apparent ΔH_{cal} for thermal unfolding; in wild-type bR it was 70.1 ± 6.8 kcal/mol, and for TGAI it was 41.7 ± 8.0 kcal/mol.

DISCUSSION

The side chains of the 25 amino acids comprising the wild-type bR carboxyl-terminus include 8 aliphatic, 4 hydroxyl, 1 aromatic, 2 basic and 5 acidic moieties, and the terminal carboxylate (*5*). It also contains 2 prolines and 3 glycines. The p*I* of the 22 amino acid bR carboxyl-terminal peptide is ~3.9. This peptide could modulate the local electrostatic environment on the cytoplasmic side of bR and influence proton uptake directly or via interactions with lipid head groups and/or bR loop region amino acids. Very limited structural information is available for putative carboxyl-terminal interactions since it is unresolved (disordered) in all X-ray structures determined to date. An NMR structure lists coordinates for the first eight amino acids of the carboxyl-terminus (*40*), four of which are maintained in the

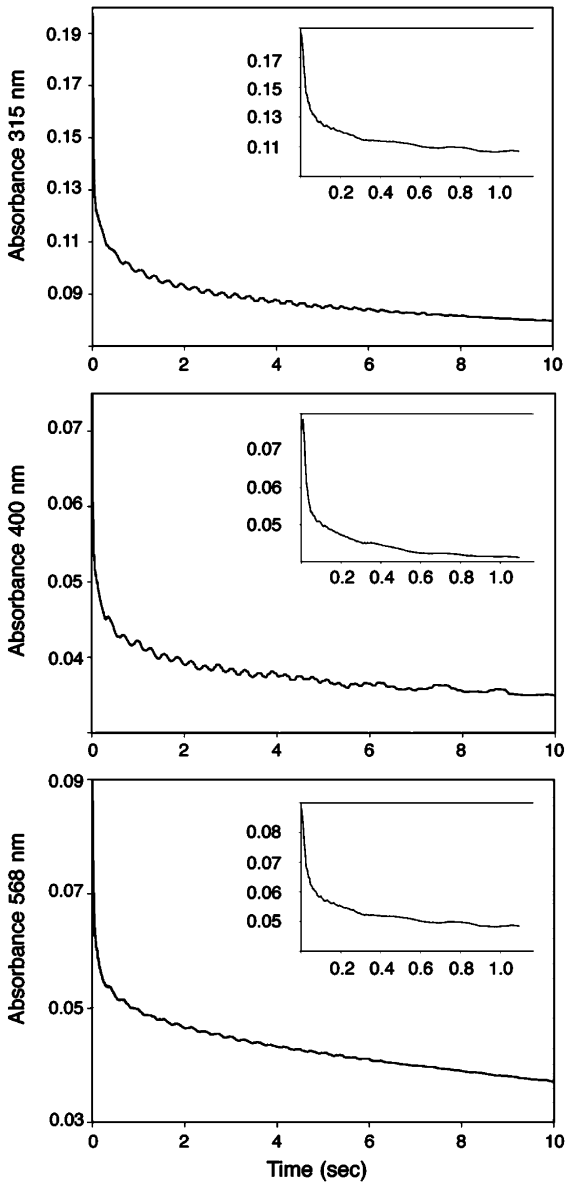

FIGURE 6: Stopped-flow analysis of TGAI denaturation by SDS. Changes in absorbance for the full truncation mutant (TGAI) following upon mixing with SDS (0.3% w/v final concentration) at 20 °C, pH 7.0. Absorbance changes at 315 nm (top panel), 400 nm (middle panel), and 568 nm (bottom panel) were recorded in separate experiments. The insets show absorbance changes out to 1 s to illustrate the fastest phase of the denaturation event.

TGAII construction. Mutagenic analysis of the roles of specific amino acids comprising the carboxyl-terminus is sparse; and the effort required for a comprehensive targeted mutagenesis would be difficult to justify based on the limited carboxyl-terminal database available. Therefore, the current study was designed to determine whether "domains" of the bR carboxyl-terminus are involved in proton pumping and protein stability. Two truncations were engineered by introduction of premature translation stop codons that removed 12 amino acids comprising a distal domain and subsequently 10 amino acids comprising a proximal domain of the carboxyl-terminus. The studies reported identify important roles in both proton recruitment and protein stability for the bR carboxyl-terminus.

Ground-State Properties and Membrane Assembly. The ground-state electrogenic environment of the bR chromophore is not influenced by the carboxyl-terminus. Both truncation mutants retinylated fully *in vivo* and exhibited light- and dark-adapted spectra over a broad pH range identical to that of wild-type. *In vitro*, at pH 7.0, the rate of dark-adaptation for the full truncation was indistinguishable from the wild-type. This is consistent with a normal tertiary fold, and normal charge distribution around the chromophore in both its *all-trans* and *13-cis* configurations. Electron diffraction, visible CD spectroscopy, and equilibrium sedimentation ultracentrifugation demonstrated that the truncation mutants formed membrane patches with trimeric lattices that are indistinguishable from those formed by wild-type bR, in agreement with earlier EM- and X-ray-diffraction (*41*) and spectroscopic (*43*) analyses of proteolytically modified bR. Since the truncations were generated genetically (not post-translational modifications as in all previous carboxyl-terminal investigations) we conclude that the carboxyl-terminus does not contribute to the *in vivo* biogenic pathway(s) accessed by wild-type bR.

Proton Pumping. Complete deletion of the carboxyl terminus radically altered the kinetics of proton uptake, while deletion of the distal 10 amino acids had essentially no effect on proton uptake. The most striking effect of complete deletion of the bR carboxyl terminus is the drastically distorted kinetics of proton uptake, as shown by the dark, right-hand trace in Figure 5C. In wild-type bR proton uptake is correlated with the decay of the M-intermediate (*2, 8, 36*) and is described by a single kinetic phase, as shown in Figure 5A and Table 1. Truncation of amino acids in the membrane proximal portion of the carboxyl-terminus resulted in two, kinetically distinct, phases of proton uptake. The first phase (85% of amplitude) was 3.7 times faster than that of wild-type proton uptake. We also observed that the major component of M decay in TGAI (~90% of amplitude) is 3.7 times faster than the corresponding component of M decay for the wild-type. Proton uptake and M decay remain coupled for the full truncation, implying that the pK_a of the carboxyl-terminal components of the proton uptake are reciprocally linked to the pK_a of D96. These results further support the idea that proton recruitment at the cytoplasmic surface of bR is coupled to M decay.

Earlier work on bR with proteinase-deleted carboxyl-termini, in reconstituted membranes and PM, produced varied results with regard to its contribution to proton pumping (*12, 13, 42, 43*). The results presented here are in agreement with the major finding of all previous studies, i.e. that removal of some-or-all of the carboxyl terminus does not prevent proton uptake and release. In some of the previous studies, proteolytic truncation of the full carboxyl-terminus resulted in a reduction of protons pumped per M-state. The authors proposed the perturbation was due to time-dependent PM aggregation of the carboxyl-terminus truncated sample (*12, 13*). Our analysis of high signal-to-noise single flash measurements of proton motion shows a clear correlation between proton uptake rates and significant perturbations of M-state formation and decay (Figure 5). To verify that PM aggregation was not affecting proton pumping of the carboxyl-terminally truncated preparations, we also performed photocycle analyses on freshly sonicated samples and observed no differences in M-state or proton pumping kinetics (data not shown). The congruence of the size of the PM sheets for both the full truncation and wild-type bR (as

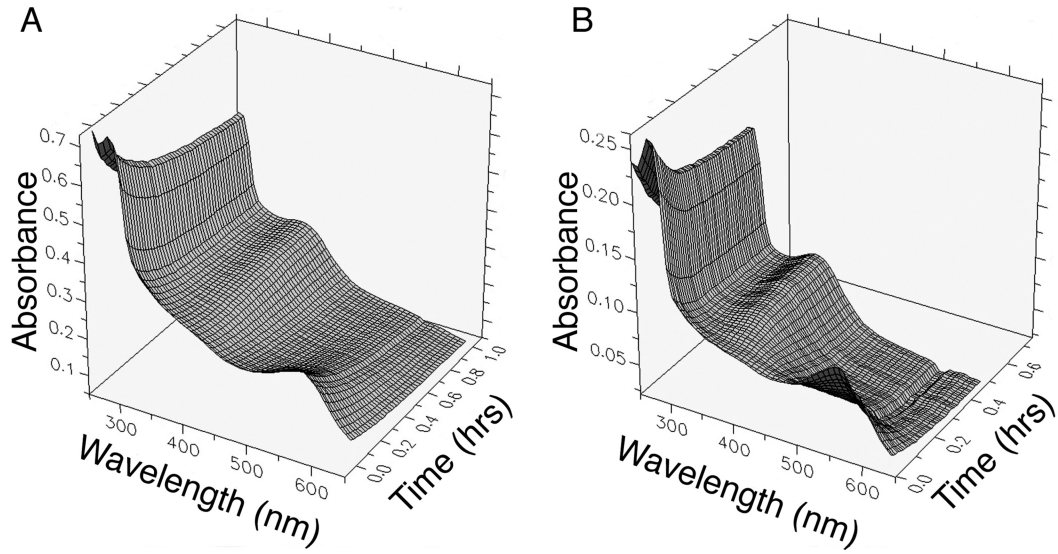

FIGURE 7: Slow kinetic analysis of the wild-type bR and TGAI denaturation by SDS. Three dimensional data sets of the time-dependent spectral changes for the wild-type bR (A) and TGAI (B) upon mixing with SDS (0.3% w/v final concentration) at 20 °C, pH 7.0. Both data sets show decreases in absorbance maxima at 280 nm (loss of light scattering as PM particles break down) and 568 nm (bR ground-state absorbance as unfolding and bleaching progresses) and an increase in absorbance at 390 nm (free retinal absorbance as unfolding, bleaching, and release of the retinaloxime progresses).

Table 2: Kinetic Analysis of bR Denaturation by SDS[a]

sample	nm	k_1	k_2	k_d
WT	568	33.0 ± 4.3	0.63 ± 0.14	$6.02 \pm 0.47 \times 10^{-4}$
	400	19.8 ± 1.7	1.32 ± 0.42	
	315	30.1 ± 1.5	0.54 ± 0.29	
TGAII	568	22.2 ± 0.3	0.29 ± 0.18	$9.63 \pm 0.50 \times 10^{-4}$
	400	41.8 ± 2.7	0.71 ± 0.37	
	315	39.2 ± 3.5	0.49 ± 0.12	
TGAI	568	35.8 ± 0.7	0.57 ± 0.16	$3.21 \pm 0.19 \times 10^{-3}$
	400	46.0 ± 3.1	0.32 ± 0.05	
	315	35.4 ± 1.9	0.16 ± 0.08	

[a] All rates are reported as s^{-1}. Solution conditions: 100 mM NaCl, titration buffer, pH 7.0, 20 °C. k_1 and k_2 are rates resolved from single wavelength stopped-flow rapid kinetic analysis. k_d is the rate of bR denaturation determined from the SVD analysis of the diode array time-dependent spectra.

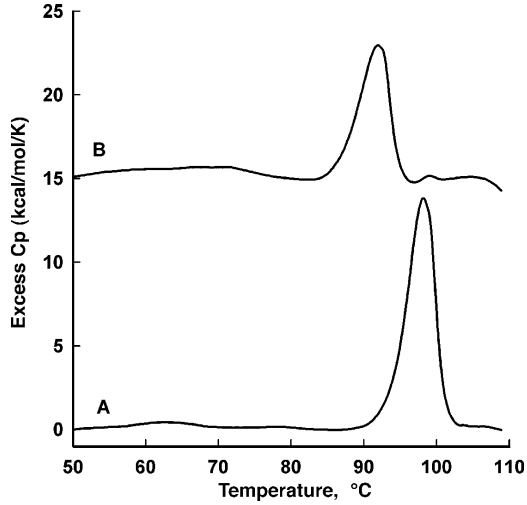

FIGURE 8: DSC thermograms of the wild-type bR and the full truncation mutant, TGAI. Typical DSC data for thermal melts of PM samples in 5 mM phosphate, pH 7.0. The scanning rate was 1.5 °C min^{-1}. (A) DSC scan of the wild-type PM. (B) DSC scan of PM containing the full-truncation mutant TGAI.

measured by analytical ultracentrifugation) also argue against sample aggregation under the experimental conditions of the current study. Thus, the present results demonstrate the proximal portion of the carboxyl terminus is required for normal kinetics of proton uptake.

The importance of long-range electrostatic coupling in bR is well established, as observed for the linkage between the pK_a's of D85 and the proton release group(s) (E194, E204 *36, 44*) and between D96 and the Schiff base (*2, 45*). The observation that the initial, dominant phases of proton uptake and M-state decay were faster following full truncation indicates that the membrane proximal portion of the wild-type protein might function to modulate proton access to the cytoplasmic half-channel. The carboxyl-terminal amine-containing side chains could repel protons, or the carboxylate-containing side chains may attract protons or form ion pairs with basic side chains, lipid head groups, or cations. Either scenario, or a combination of both, could serve to modulate the pK_a's of acceptor groups located in close proximity to the cytoplasmic proton channel.

Proton recruitment by bR is complex, with components originating from amino acid moieties (hypothesized to include numerous carboxylates located in interhelical loop regions) and from bulk protons (*4*). Limited mutagenic analyses indicate that regulation of proton recruitment can involve arginine 227, glycine 231, and glutamic acid 234, all located in membrane proximal domain of the carboxyl-terminal peptide (*7*−*9*). We note that proton uptake in TGAI is composed of two kinetic components, only the first of which corresponds to M decay. The perturbation introduced by TGAI may have altered bulk proton uptake from post M-state intermediates, reflected in the very slow second phase of proton uptake observed in TGAI. Alternatively, a population of TGAI may relax to an alternate (and unidentified) conformational state characterized by slow proton uptake. Another alternative is that some, or all, of the five carboxyl-terminal side chains containing carboxylates are direct components of a putative proton antenna. As previously shown for proton release (*36*), it is likely that multiple

reprotonation pathways exist to ensure that the pumping cycle is completed under various solution conditions.

The coupled reactions leading to proton translocation appear to be remarkably complex. We observed that the full carboxyl-terminal truncation also had a small affect on the rate of formation of M. M formation coincides with deprotonation of the Schiff base and release of a proton to the extracellular media (*1, 2, 46*). Perturbations introduced by truncating the cytoplasmic carboxyl-terminus propagated to the extracellular side of the protein, the site of the proton release group. A body of previous work indicates that regulation of proton motion involves a complex set of intermolecular interactions. For example, R82 is a residue in helix C and a component of the complex hydrogen-bonding network involved in regulating the pK_a of the Schiff base counterion (D85) and the pK_a of the proton release group (*7, 8, 36*). Mutation R82Q perturbs the electrostatic environment of the Schiff base and the coupling to the extracellular release group(s). Mutation of glycine 231 (G231C) reverted the perturbed photomechanism of R82A to wild-type (*8*). In addition, mutation of arginine 227 (R277Q), a carboxyl-terminal amino acid immediately upstream of the translation stop codon introduced in TGAI, resulted in a decrease in the rate of M decay (*7*). R227 is the terminal amino acid in TGAI while G231 has been deleted. Either R227 cannot compensate for the pumping perturbation introduced by TGAI or the proximity of the terminal carboxylate may perturb the R227 pK_a, altering its electrostatic contribution. Dencher and colleagues suggested that E234 may be a critical component of a complex cytoplasmic proton counterion in the bR ground-state (*9*). E234 is deleted in TGAI. The demonstration that R227, G231 and E234 contribute to the proton pumping mechanism is consistent with our interpretation that the proximal region of the carboxyl-terminus is likely linked to the reprotonation mechanism. Taken in sum, these observations suggest that long-range coupling between extracellular and intracellular domains plays a fundamental role in formation of M. The three carboxylate-containing side chains removed in TGAI represent obvious targets for future site-directed studies.

bR Structural Stability. Early investigations focused on the structure of the wild-type bR carboxyl-terminus indicated that it was disordered, mobile, and/or occupied multiple structural positions within the time course of EM- and X-ray-diffraction experiments (*41*). Most relevant to the current work, deletion of the carboxyl-terminus appeared to result in small rearrangements of helices near the site of attachment, at least at the cytoplasmic side of helix G (*41*) indicating a possible carboxyl-terminus-helical bundle interaction. Subsequent fluorescence labeling, accessibility to papain cleavage, fluorescence polarization, and NMR experiments indicated that the carboxyl-terminus was segmented. The carboxyl-terminus was proposed to contain a distal domain that was highly mobile and a transiently structured proximal domain (*11, 47*). The current work demonstrates that the carboxyl-terminus is comprised of two structural and functional domains.

SDS Denaturation. Comparison of the denaturation reactions of wild-type bR to those of bR mutants affords insight into the contributions of individual amino acids, or amino acids domains, to overall protein stability (*48, 49*). We have used this strategy to evaluate the carboxyl-terminal contribution to bR stability. In the current study, we observed two rapid, well-resolved phases attributable to SDS:PM interactions for all bR constructions. These kinetic unfolding experiments are consistent with established mechanisms of protein denaturation by SDS which show that the denaturation reactions involve rapid micelle binding (*50*), weakening of core protein interactions (*51*), and subsequent protein unfolding. In the current study involving purple membranes, the fastest phases were well resolved (Figure 6, Table 2), whereas for the majority of other studies SDS−micelle or SDS−protein interaction occurred in the dead time of the mixing experiments. The PM is an extremely dense lipid: bR assembly and as a consequence SDS interactions occur on a milliseconds time scale rather than submilliseconds as observed for pure protein and mixed micelle systems. The bR → bO denaturation reactions observed (loss of A_{568}, or gain in A_{390}) were best described by a single exponential decay; arguing against unfolding intermediates for any of the bR's in this study. Intermediates may exist, but the scattering component of the PM denaturation may mask their existence. Alternatively, folding intermediates could be spectrally silent. The apparent lack of unfolding intermediates simplified the relevant experimental interpretation. Whether intermediates exist or not, it is clear that removal of the carboxyl-terminus accelerated the rate of bR unfolding indicating that carboxyl-terminal interactions add structural stability to bR.

A different measure of bR stability is evaluated by thermal denaturation, as monitored by DSC. The T_m and apparent calorimetric enthalpy of thermal denaturation of bR (in the PM) in water (*37*) agrees well with our results in 5 mM phosphate, pH 7.0. Wild-type bR reconstituted in phospholipids or mixed micelles exhibited reductions in both T_m and ΔH_{cal}, an indication that interactions of monomers within the bR trimer and/or the lipids of the PM constrain bR structural stability. In the current work we show that the T_m and apparent ΔH_{cal} of the denaturation transition were both lowered upon removal of the carboxyl-terminus, demonstrating that removal of the carboxyl-terminus reduces the thermal stability of bR, even when assembled as trimers within the PM (Figure 8). As observed previously, there is no change in ΔCp for the denaturation transition (*37, 39*). While the mechanisms for SDS and temperature denaturation are different, both approaches demonstrate that the carboxyl-terminus contributes significantly to bR global stability.

bR structure−function relationships have been conceptually dominated by molecular interactions within the transmembrane helical bundle. Even the folding paradigm is dominated by intramembranous helix interactions; formation of secondary structures (helices) followed by collapse in to tertiary structures (helix bundles) (*56*−*60*). Early studies may have contributed to this view since bR function (and therefore structure) appeared to be tolerant to loop region insertions (*16, 18, 61*), deletions (*62*), and fragmentation (*14, 15*). In nonnative detergent and lipid systems the majority of loop region perturbations supported proton pumping (albeit some with significantly reduced efficiency). However, dependent on the reconstitution system used, five of the six loop regions (A/B, B/C, C/D, E/F and E/G) have been shown to be sensitive to amino acid replacement (*16*−*18*). Therefore loop regions impact bR folding and function, possibly by constraining helix orientations. The current work illustrates that the extramembranous and intracellular carboxyl-terminus also

contributes to bR structural stability and functional integrity. While removal of the carboxyl-terminus results in the formation of near-native tertiary structure (consistent with earlier work (*43*)) important (and transient) interactions with the helical bundle must be perturbed, resulting in structural instability and perturbations of the proton pumping mechanism.

In summary, the results presented here indicate that the carboxyl-terminus interacts with the bR transmembrane helical bundle to achieve its final folded state. Perturbation of the carboxyl-terminus did not alter the ground-state chromophoric properties, thus putative carboxyl-terminal interactions do not propagate into the chromophore-binding pocket, in agreement with earlier investigations of proteinase truncated PM (*43*). This gives the impression of a folded core with a stability that is somewhat independent of the rest of the helical bundle. These results are consistent with earlier suggestions that a rigid core exists that constrains retinal stereochemistry (*40, 52*). Interactions between the helix bundle and the carboxyl-terminus are likely to be electrostatic in nature. Numerous carboxyl-terminal side chains can participate as hydrogen bond acceptors or as cations in ion pairing interactions. As assessed by the SDS denaturation experiments, both TGAI and TGAII showed reduced stability, thus the full carboxyl-terminus influences overall protein stability. However, truncation of the distal end did not affect light-activated proton pumping. In contrast, amino acids in the proximal domain appeared to contribute in the recruitment of protons to the intracellular proton channel orifice (*3, 4*). The work presented here indicates that the bR carboxyl-terminal coding region participates in proton pumping and stability, the structural correlates of which remain to be determined.

The vast majority of bR structural studies have relied on the phenomenal success of X-ray crystallography, but in all structures to date the carboxyl-terminus is unstructured. Therefore, mechanistic contributions attributed to the bR carboxyl-terminus cannot be determined crystallographically. An alternative to evaluating the carboxyl-terminal structure in wild-type bR is to determine the structure of the helical bundle in the absence of the carboxyl-terminus. Any differences observed may point to sites of carboxyl-terminal interaction. We have pursued characterization of the X-ray crystallographic structure of TGAI. To date, TGAI crystals belonging to the space group *P*21 diffract to 3.5 Å but the structure has resisted solution (A. Goldman and V.-P. Jaakola, personal communication).

While the current study does not allow identification of the individual amino acids involved, the *in vivo* truncation strategy afforded an efficient and comprehensive probing of the bR carboxyl-terminal coding region. This first pass analysis will serve to focus future higher resolution site-directed mutagenesis that can determine the individual contributions of carboxyl-terminal amino acids in proton recruitment and structural stability.

ACKNOWLEDGMENT

The authors thank Dr. S. Kelty and S. Stoehr for critical reading of the manuscript.

SUPPORTING INFORMATION AVAILABLE

A summary of the SVD analysis of the SDS denaturation experiments can be found in Figure 1S (wild-type bR) and Figure 2S (TGAI). This material is available free of charge via the Internet at http://pubs.acs.org.

REFERENCES

1. Oesterhelt, D. (1998) The structure and mechanism of the family of retinal proteins from halophilic archaea. *Curr. Opin. Struct. Biol. 8*, 489–500.
2. Lanyi, J. K. (1998) Understanding structure and function in the light-driven proton pump bacteriorhodopsin. *J. Struct. Biol. 124*, 164–178.
3. Kimura, Y., Vassylyev, D. G., Miyazawa, A., Kidera, A., Matsushima, M., Mitsuoka, K., Murata, K., Hirai, T., and Fujiyoshi, Y. (1997) Surface of bacteriorhodopsin revealed by high-resolution electron crystallography. *Nature 389*, 206–211.
4. Checover, S., Nachliel, E., Dencher, N. A., and Gutman, M. (1997) Mechanism of proton entry into the cytoplasmic section of the proton-conducting channel of bacteriorhodopsin. *Biochemistry 36*, 13919–13928.
5. Dunn, R., McCoy, J., Simsek, M., Majumdar, A. S. C., RajBhandary, U., and Khorana, H. G. (1981) The bacteriorhodopsin gene. *Proc. Natl. Acad. Sci. U.S.A. 78*, 6744–6748.
6. Grigorieff, N., Ceska, T. A., Downing, K. H., Baldwin, J. M., and Henderson, R. (1996) Electron-crystallographic refinement of the structure of bacteriorhodopsin. *J. Mol. Biol. 259*, 393–421.
7. Stern, L. J., and Khorana, H. G. (1989) Structure-function studies on bacteriorhodopsin. X. Individual substitutions of arginine residues by glutamine affect chromophore formation, photocycle, and proton translocation. *J. Biol. Chem. 264*, 14202–14208.
8. Alexiev, U., Mollaaghababa, R., Khorana, H. G., and Heyn, M. P. (2000) Evidence for long range allosteric interactions between the extracellular and cytoplasmic parts of bacteriorhodopsin from the mutant R82A and its second site revertant R82A/G231C. *J. Biol. Chem. 275*, 13431–13440.
9. Checover, S., Marantz, Y., Nachliel, E., Gutman, M., Pfeiffer, M., Tittor, J., Oesterhelt, D., and Dencher, N. A. (2001) Dynamics of the proton transfer reaction on the cytoplasmic surface of bacteriorhodopsin. *Biochemistry 40*, 4281–4292.
10. Brown, L. S. (2000) Reconciling crystallography and mutagenesis: a synthetic approach to the creation of a comprehensive model for proton pumping by bacteriorhodopsin. *Biochim. Biophys. Acta 1460*, 49–59.
11. Renthal, R., Dawson, N., Tuley, J., and Horowitz, P. (1983) Constraints on the flexibility of bacteriorhodopsin's carboxyl-terminal tail at the purple membrane surface. *Biochemistry 22*, 5–12.
12. Govindjee, R., Ohno, K., Chang, C. H., and Ebrey, T. G. (1984) The C-terminal tail of bacteriorhodopsin-its conformation and role in proton pumping. *Prog. Clin. Biol. Res. 164*, 13–25.
13. Ovchinnikov, Y., Abdulqaev, N., Kiselev, A., Drachev, L., Kaulen, A., and Shulachev, V. P. (1986) The water-exposed C-terminal sequence of bacteriorhodopsin does not alter H+ pumping. *FEBS 194* (1), 16–20.
14. Liao, M. J., London, E., and Khorana, H. G. (1983) Regeneration of the native bacteriorhodopsin structure from two chymotryptic fragments. *J. Biol. Chem. 258*, 9949–9955.
15. Huang, K. S., Bayley, H., Liao, M. J., London, E., and Khorana, H. G. (1981) Refolding of an integral membrane protein. Denaturation, renaturation, and reconstitution of intact bacteriorhodopsin and two proteolytic fragments. *J. Biol. Chem. 256*, 3802–3809.
16. Teufel, M., Pompejus, M., Humbel, B., Friedrich, K., and Fritz, H. J. (1993) Properties of bacteriorhodopsin derivatives constructed by insertion of an exogenous epitope into extra-membrane loops. *EMBO J. 12*, 3399–3408.
17. Allen, S. J., Kim, J. M., Khorana, H. G., Lu, H., and Booth, P. J. (2001) Structure and function in bacteriorhodopsin: the effect of the interhelical loops on the protein folding kinetics. *J. Mol. Biol. 308*, 423–435.
18. Kim, J. M., Booth, P. J., Allen, S. J., and Khorana, H. G. (2001) Structure and function in bacteriorhodopsin: the role of the interhelical loops in the folding and stability of bacteriorhodopsin. *J. Mol. Biol. 308*, 409–422.
19. Turner, G. J., Reusch, R., Winter-Vann, A. M., Martinez, L., and Betlach, M. C. (1999) Heterologous gene expression in a membrane-protein-specific system. *Protein Expression Purif. 17*, 312–323.
20. Wagner, G., Oesterhelt, D., Krippahl, G., and Lanyi, J. (1983) Bioenergetic role of halorhodopsin in *Halobacterium halobium* cells. *FEBS Lett. 131*, 341–345.

21. DasSarma, S., and Fleischmann, E. M. (1995) in *Archaea, A laboratory manual* (Robb, F. T., Ed.) pp 1−280, Cold Spring Harbor Laboratory Press, Cold Spring Harbor.
22. Cline, S. W., Schalkwyk, L., and Doolittle, W. F. (1989) Transformation methods for halophilic archeabacteria. *J. Bacteriol. 171*, 4987–4991.
23. Winter-Vann, A. M., Martinez, L., Parker, L., Talbot, J., and Turner, G. J. (1999) Transgenic stability of membrane protein expression in *Halobacterium salinarum*. *Cancer Res. Ther. Control 8*, 275–289.
24. Winter-Vann, A. M., Martinez, L., Bartus, C., Levay, A., and Turner, G. J. (2001) G protein-coupled receptor expression in Halobacterium salinarum, in *Perspectives on Solid State NMR in Biology* (Kiihne, S., and de Groot, H. J. M., Eds.) pp 141−160, Kluwer, Dordrecht, The Netherlands, Leiden.
25. Oesterhelt, D., and Stoeckenius, W. (1974) Isolation of the cell membrane of *Halobacterium halobium* and its fractionation into red and purple membrane. *Methods Enzymol. 31*, 667–678.
26. Rehorek, M., and Heyn, M. P. (1979) Binding of all-trans retinal to the purple membrane. Evidence for cooperativity and determination of the extinction coefficient. *Biochemistry 18*, 4977–4983.
27. Philo, J. S. (2006) Improved methods for fitting sedimentation coefficient distributions derived by time-derivative techniques. *Anal. Biochem. 354*, 238–246.
28. Mitra, A. K., Miercke, L., Turner, G., Shand, R., Betlach, M. C., and Stroud, R. (1993) Two-dimensional Crystallization of Escherichia coli-expressed Bacteriorhodopsin and Its D96N Variant: High Resolution Structural Studies in Projection. *Biophys. J. 65*, 1295–1306.
29. London, E., and Khorana, H. G. (1982) Denaturation and renaturation of bacteriorhodopsin in detergents and lipid-detergent mixtures. *J. Biol. Chem. 257*, 7003–7011.
30. Mitchell, D. C., Niu, S. L., and Litman, B. J. (2001) Optimization of receptor-G protein coupling by bilayer lipid composition I: kinetics of rhodopsin-transducin binding. *J. Biol. Chem. 276*, 42801–42806.
31. Frasier, S., and Johnson, M. (1985) Nonlinear least squares analysis. *Methods Enzymol. 117*, 301–342.
32. Faham, S., and Bowie, J. U. (2002) Bicelle crystallization: a new method for crystallizing membrane proteins yields a monomeric bacteriorhodopsin structure. *J. Mol. Biol. 316*, 1–6.
33. Miercke, L. J. W., Ross, P. E., Stroud, R. M., and Dratz, E. A. (1989) Purification of bacteriorhodopsin and characterization of mature and partially processed forms. *J. Biol. Chem. 264*, 7531–7535.
34. Heyn, M. P., Bauer, P. J., and Dencher, N. A. (1975) A natural CD label to probe the structure of the purple membrane from Halobacterium halobium by means of exciton coupling effects. *Biochem. Biophys. Res. Commun. 67*, 897–903.
35. Scherrer, P., Mathew, M. K., Sperling, W., and Stoeckenius, W. (1989) Retinal isomer ratio in dark-adapted purple membrane and bacteriorhodopsin monomers. *Biochemistry 28*, 829–834.
36. Balashov, S. P., Imasheva, E. S., Govindjee, R., and Ebrey, T. G. (1996) Titration of aspartate-85 in bacteriorhodopsin: what it says about chromophore isomerization and proton release. *Biophys. J. 70*, 473–481.
37. Jackson, M. B., and Sturtevant, J. M. (1978) Phase transitions of the purple membranes of *Halobacterium halobium*. *Biochemistry 17*, 911–915.
38. Brouillette, C. G., McMichens, R. B., Stern, L. J., and Khorana, H. G. (1989) Structure and thermal stability of monomeric bacteriorhodopsin in mixed phospholipid/detergent micelles. *Proteins 5*, 38–46.
39. Brouillette, C. G., Muccio, D. D., and Finney, T. K. (1987) pH dependence of bacteriorhodopsin thermal unfolding. *Biochemistry 26*, 7431–7438.
40. Patzelt, H., Simon, B., terLaak, A., Kessler, B., Kuhne, R., Schmieder, P., Oesterhelt, D., and Oschkinat, H. (2002) The structures of the active center in dark-adapted bacteriorhodopsin by solution-state NMR spectroscopy. *Proc. Natl. Acad. Sci. U.S.A. 99*, 9765–9770.
41. Wallace, B. A., and Henderson, R. (1982) Location of the carboxyl terminus of bacteriorhodopsin in purple membrane. *Biophys. J. 39*, 233–239.
42. Govindjee, R., Ohno, K., and Ebrey, T. G. (1982) Effect of the removal of the COOH-terminal region of bacteriorhodopsin on its light-induced H+ changes. *Biophys. J. 38*, 85–87.
43. Liao, M. J., and Khorana, H. G. (1984) Removal of the carboxyl-terminal peptide does not affect refolding or function of bacteriorhodopsin as a light-dependent proton pump. *J. Biol. Chem. 259*, 4194–4199.
44. Balashov, S. P., Lu, M., Imasheva, E. S., Govindjee, R., Ebrey, T. G., Othersen, B., 3rd, Chen, Y., Crouch, R. K., and Menick, D. R. (1999) The proton release group of bacteriorhodopsin controls the rate of the final step of its photocycle at low pH. *Biochemistry 38*, 2026–2039.
45. Balashov, S. P. (2000) Protonation reactions and their coupling in bacteriorhodopsin. *Biochim. Biophys. Acta 1460*, 75–94.
46. de Groot, H. J., Smith, S. O., Courtin, J., van den Berg, E., Winkel, C., Lugtenburg, J., Griffin, R. G., and Herzfeld, J. (1990) Solid-state 13C and 15N NMR study of the low pH forms of bacteriorhodopsin. *Biochemistry 29*, 6873–6883.
47. Yamaguchi, S., Tuzi, S., Seki, T., Tanio, M., Needleman, R., Lanyi, J. K., Naito, A., and Saito, H. (1998) Stability of the C-terminal α-helical domain of bacteriorhodopsin that protrudes from the membrane surface, as studied by high-resolution solid-state 13C NMR. *J. Biochem. (Tokyo) 123*, 78–86.
48. Lau, F. W., and Bowie, J. U. (1997) A method for assessing the stability of a membrane protein. *Biochemistry 36*, 5884–5892.
49. Chen, G. Q., and Gouaux, E. (1999) Probing the folding and unfolding of wild-type and mutant forms of bacteriorhodopsin in micellar solutions: evaluation of reversible unfolding conditions. *Biochemistry 38*, 15380–15387.
50. Otzen, D. E. (2002) Protein unfolding in detergents: effect of micelle structure, ionic strength, pH, and temperature. *Biophys. J. 83*, 2219–22130.
51. Otzen, D. E., and Oliveberg, M. (2002) Burst-phase expansion of native protein prior to global unfolding in SDS. *J. Mol. Biol. 315*, 1231–1240.
52. Reat, V., Patzelt, H., Ferrand, M., Pfister, C., Oesterhelt, D., and Zaccai, G. (1998) Dynamics of different functional parts of bacteriorhodopsin: H-2H labeling and neutron scattering. *Proc. Natl. Acad. Sci. U.S.A. 95*, 4970–4975.
53. Lee, D. C., Herzyk, E., and Chapman, D. (1987) Structure of Bacteriorhodopsin investigated using fourier transform infrared spectroscopy and proteolytic digestion. *Biochemistry 26*, 5775–5783.
54. Abdulaev, N. G., Feigina, M. Y., Kiselev, A. V., Ovchinnikov, Y. A., Drachev, L. A., Kaulen, A. D., Khitrina, L. V., and Skulachev, V. P. (1978) Products of limited proteolysis of bacteriorhodopsin generate a membrane potential. *FEBS Lett. 90*, 190–194.
55. Kimura, K., Mason, T. L., and Khorana, H. G. (1982) Immunological probes for bacteriorhodopsin. Identification of three distinct antigenic sites on the cytoplasmic surface. *J. Biol. Chem. 257*, 2859–2867.
56. Popot, J., and Engleman, D. M. (1990) Membrane protein folding and oligomerization: the two-stage model. *Biochemistry 29*, 4031–4037, No. 17.
57. Riley, M. L., Wallace, B. A., Flitsch, S. L., and Booth, P. J. (1997) Slow α helix formation during folding of a membrane protein. *Biochemistry 36*, 192–196.
58. Booth, P. J., Riley, M. L., Flitsch, S. L., Templer, R. H., Farooq, A., Curran, A. R., Chadborn, N., and Wright, P. (1997) Evidence that bilayer bending rigidity affects membrane protein folding. *Biochemistry 36*, 197–203.
59. Bowie, J. U. (1997) Helix packing in membrane proteins. *J. Mol. Biol. 272*, 780–789.
60. Engelman, D. M., Chen, Y., Chin, C. N., Curran, A. R., Dixon, A. M., Dupuy, A. D., Lee, A. S., Lehnert, U., Matthews, E. E., Reshetnyak, Y. K., Senes, A., and Popot, J. L. (2003) Membrane protein folding: beyond the two stage model. *FEBS Lett. 555*, 122–125.
61. Abdulaev, N. G., Strassmaier, T. T., Ngo, T., Chen, R., Luecke, H., Oprian, D. D., and Ridge, K. D. (2002) Grafting segments from the extracellular surface of CCR5 onto a bacteriorhodopsin transmembrane scaffold confers HIV-1 coreceptor activity. *Structure (Cambridge) 10*, 515–525.
62. Gilles-Gonzalez, M. A., Engleman, D. M., and Khorana, H. G. (1991) Structure-Function Studies of Bacteriorhodopsin XV Effects of Deletions in Loops B-C and E-F on Bacteriorhodopsin Chromophore and Structure. *J. Biol. Chem. 266* (13), 8545–8550.

BI801799J